

# Adaptive Dictionary-Based Spatio-Temporal Flow Estimation for Echo PIV

Ecaterina Bodnariuc<sup>\*1</sup>, Arati Gurung<sup>2</sup>, Stefania Petra<sup>1\*\*</sup>, and Christoph Schnörr<sup>\*1</sup>

<sup>1</sup> Image and Pattern Analysis Group, University of Heidelberg, Germany  
ecaterina.bodnariuc@iwr.uni-heidelberg.de,  
{petra,schnoerr}@math.uni-heidelberg.de

<sup>2</sup> Laboratory for Aero and Hydrodynamics (3ME-P&E), Delft University of Technology, The Netherlands  
a.gurung@tudelft.nl

**Abstract.** We present a novel approach to detect the trajectories of particles by combining (a) adaptive dictionaries that model physically consistent spatio-temporal events, and (b) convex programming for sparse matching and trajectory detection in image sequence data. The mutual parametrization of these two components are mathematically designed so as to achieve provable convergence of the overall scheme to a fixed point. While this work is motivated by the task of estimating instantaneous vessel blood flow velocity using ultrasound image velocimetry, our contribution from the optimization point of view may be of interest also to related pattern and image analysis tasks in different application fields.

**Keywords:** motion estimation, fixed point algorithm, adaptive dictionaries, sparse representation, sparse error correction, Echo PIV

## 1 Introduction

**Overview.** *Ultrasound Image Velocimetry (Echo PIV)* has evolved into an active research interest primarily due to its ability to measure instantaneous flow velocity and wall shear stress in a non-intrusive manner [1,2] with a wide range of applications (e.g. from arterial wall shear stress measurements for atherosclerosis-related studies to two-phase flow quantification for industrial studies such as dredging).

Currently available sensors, however, severely limit the spatial and temporal resolution of measurements. Computational cross-correlation techniques, adopted from the traditional laser-based optical PIV and used in different fields of experimental fluid mechanics [3], suffer from poor signal to noise in the reconstructed image sequences. Moreover, the established cross-correlation methods make it difficult to mathematically quantify motion information over an entire

---

\* EB and CS appreciate financial support by the German Research Foundation (DFG).

\*\* SP acknowledges financial support by the Ministry of Science, Research and Arts, Baden-Württemberg, within the Margarete von Wrangell postdoctoral lecture qualification program.

image sequence in a consistent frame-by-frame analysis of the spatio-temporal flow characteristics. As such, it becomes important, but yet challenging, to incorporate the physical principles governing the imaged fluid flow.

In this paper we present a novel approach that directly addresses these shortcomings in terms of adaptive spatio-temporal dictionaries of particle trajectories. These dictionaries are based on a basic physical model of vessel blood flow and are integrated into a standard sparse convex programming framework.

**Related Work, Contribution.** Research in connection with Echo PIV concerns (i) sensor design image reconstruction and (ii) image analysis. Since research on sensor design is rapidly evolving [4,5], we ignore this inverse modelling aspect and focus on (ii) with context to PIV wherein we derive a *mathematical abstraction of “particles”, to be understood as coefficients of a basis expansion, that discretises a realistic imaging operator in our future work.*

Echo PIV employs the standard cross-correlation technique for motion estimation [1,2]. In this paper, we propose a novel approach radically different from this standard protocol with the following objectives:

1. Any imaging operator model discretized by suitable basis functions can be incorporated later on.
2. Particle trajectories are detected by a comprehensive spatio-temporal analysis of entire image sequences in terms of dictionaries of trajectories. This copes better with noise in comparison to techniques that merely analyse subsequent image pairs. Furthermore, physical models of vessel blood flow [6,7] can be directly exploited.
3. The computational costs for the aforementioned spatio-temporal analysis are subdivided by adapting a smaller collection of dictionaries until convergence.

While the novelty of our approach is obvious from the viewpoint of Echo PIV, our main contribution from the optimization point of view concerns the *consistent integration of adaptive dictionaries* into a standard sparse convex programming framework. This is accomplished by carefully modelling the mutual interaction of dictionary parametrization and sparse convex particle matching so as to obtain a provably converging fixed point scheme. These mathematical aspects of our approach might be of interest also to related computational image and pattern analysis tasks in different application fields.

**Organization.** The application and the corresponding imaging techniques are sketched in Section 2. Section 3 details the model-based definition of dictionaries together with the variational approach for motion estimation through particle trajectory detection. Section 4 provides a convergence analysis of the adaptive variational approach. Properties of our approach are validated experimentally in Section 5.

**Basic Notation.** We set  $[n] = \{1, 2, \dots, n\}$  for  $n \in \mathbb{N}$ . Vectors are column vectors and indexed by superscripts.  $\langle x, z \rangle$  denotes the standard scalar product in  $\mathbb{R}^n$ , and  $\|x\|_1 = \sum_{i=1}^n |x_i|$  and  $\|x\| := \|x\|_2 = \sqrt{\sum_{i=1}^n x_i^2}$ .  $\mathbb{1} = (1, 1, \dots, 1)^\top$

denotes the one-vector whose dimension will always be clear from the context.  $\Delta_d = \{x \in \mathbb{R}_+^d : \langle \mathbb{1}, x \rangle = 1\}$  denotes the probability simplex in  $\mathbb{R}^d$ .

## 2 Ultrasound Imaging and Echo PIV

We briefly sketch the state-of-the-art in imaging and motion analysis in Echo PIV to highlight the novelty of our own methodological approach compared to the established computational PIV techniques.

**Particle Image Velocimetry (PIV).** *PIV* is an optical method for measuring fluid flows. For the purpose of imaging, the fluid is seeded with particles that follow the flow dynamics. The region of interest is illuminated with a laser sheet and a high-speed camera takes successive images. In a subsequent step, a cross correlation technique is applied to every pair of two subsequent images and returns an estimate of the instantaneous velocity field. For a recent overview of the history of PIV techniques, we refer to [8].

**Ultrasound Microbubble Imaging.** *Echo PIV*, first introduced in [1], is a

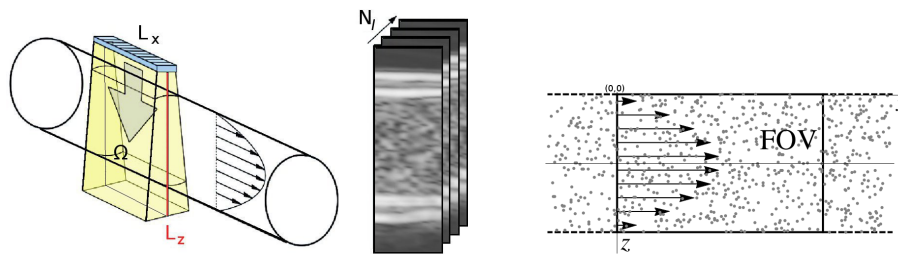


**Fig. 1.** A schematic representation of an Echo PIV setup. The left image, adapted from [2], overviews geometry and orientation of the transducer. Velocity is estimated from a sequence of B-mode images (middle). Flow motion is estimated from the motion of tracer particles injected in the medium (right), which follow the flow dynamics – here, a steady laminar flow.

technique based on the same PIV principles. Instead of the high-speed cameras used in optical PIV, an *ultrasound transducer* is used in Echo PIV to capture tracer images with the ability to image opaque media. Another major difference to optical 2D PIV is the generation of so-called *B-mode* images, as sketched in Figures 1 and 2. These 2D images are acquired via the conventional pulse-echo technique that concatenates a series of scan lines within the field of view (FOV), as depicted in Fig. 2. This severely limits the spatio-temporal resolution of flow measurements.

One way to overcome this problem is to replace multiple line measurements by a single *plane wave* illumination of the medium [4]. *Plane wave imaging* was very recently applied to Echo PIV [5] and allows for measuring higher velocities,

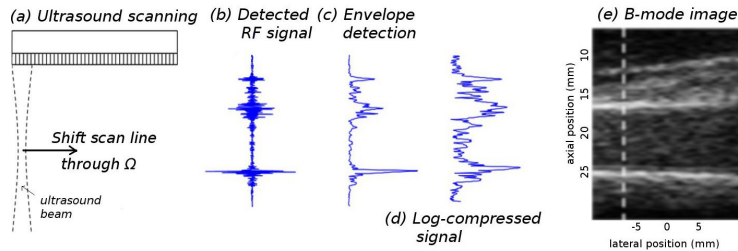


**Fig. 2.** B-mode imaging in Echo PIV: images are not recorded as snapshots, but are usually constructed line-by-line, due to the shifting of the ultrasound beam (a). The data – RF signals (b) – can be converted (offline) to so-called B-mode images (e) by means of envelope detection (c) and log compression (d). This scanning procedure results in a blurred, smeared image due to moving particles between consecutive measurements.

since the frame rate is only limited by the propagation time of the waves, rather than by the number of consecutive measurements necessary to obtain a single B-mode image. *This motivates us to ignore inter-line delay in our present work.*

**Motion Estimation.** Standard Echo PIV setups estimate the velocity field by matching image patterns across consecutive image pairs within the acquired image sequence, as in conventional PIV [8,9]. Such PIV methods fail to

- (i) exploit the entire spatio-temporal context of a corresponding volume of image sequence data, and
- (ii) take into account the physical prior knowledge in a mathematically more principled way.

Our present work addresses both aspects for the specific setting of Echo PIV as summarized in Section 1.

### 3 Spatio-Temporal Motion Model and Estimation

#### 3.1 Dictionary of Moving Particles

As mentioned in Section 2, ultrasound images of the seeded flow for Echo PIV are composed of vertical scan lines within the FOV acquired at different time steps. This scheme limits the frame rate and consequently the maximum resolvable velocity. In the present work, we propose a different acquisition protocol motivated by current research on image acquisition [4,5] in which the whole image/frame is recorded at the same point in time.

With index  $n$  we label the image of the FOV recorded at time  $\tau_n = (n-1) \Delta t$ ,  $n \in [N_I]$ , where  $N_I$  is the total number of frames. All images have size  $L_x \times L_z$  in length units or  $l_x \times l_z$  in pixels. We introduce a 2D rectangular grid with lattice spacing  $\Delta x = L_x/l_x$ ,  $\Delta z = L_z/l_z$  in  $x$  and  $z$  respectively in the plane of FOV, induced by discrete pixel representation of images.

Below we describe how to build a flow dictionary corresponding to steady laminar flow with maximal velocity along the cylinder axis equal to  $v_m$ .

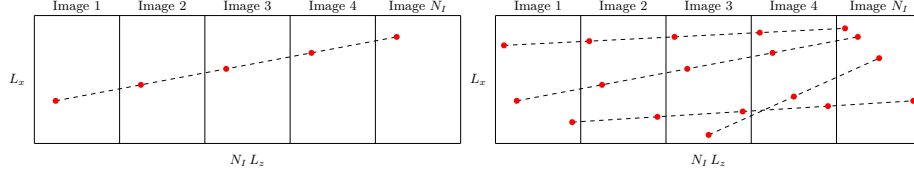


**Fig. 3.** Each column of the dictionary  $D$  is an image of an undersampled discrete line, and describes a possible trajectory in the  $N_I$  acquired images concatenated along the tube axis (left). Each such column depends on the discretization of  $\Omega$ , acquisition process and flow model. Here the Poiseuille flow model leads to straight lines. The input data (right) is given by all  $N_I$  frames concatenated along the tube axis. The problem is to *sparingly* match *imaged* particles to trajectories in  $D$  parametrized by the unknown maximal velocity  $v_m$ .

**Dictionary of a single velocity profile.** The dictionary of trajectories  $D$  is a sparse matrix with binary entries  $\{0, 1\}$  and it describes the position of particles at time  $\tau_n$ ,  $n \in [N_I]$  relative to the FOV. Each column in  $D$  is associated to the trajectory of a single particle  $j$ ,  $j \in [N_P]$ , where  $N_P$  denotes the number of particles. The number of columns in  $D$  equals the number of possible trajectories. Due to the discretization, in the limit when a particle is located at all grid points, there is an upper bound for  $N_P < l_x l_z + (N_I - 1) \Delta t v_m l_x L_x / l_z$ . The number of rows in  $D$  is independent of  $v_m$  and equals  $N_I l_x l_z$ .

According to the adopted model sketched in Figure 1 (right panel), the motion of particle  $j$  with initial coordinates  $(x_1^j, z_1^j)$  at time  $\tau_1$  is governed by

$$\begin{cases} x_n^j = x_1^j + (n-1)\Delta t v_m \left(1 - \left(\frac{r^j}{R}\right)^2\right), \\ z_n^j = z_1^j = \text{const.} \end{cases} \quad (1)$$

where  $r^j = |z_1^j - R|$ ,  $z_1^j \in [0, 2R]$  is the distance from the axis and  $R$  the inner radius  $R$  of the cylinder.

If at time  $\tau_n$  particle  $j$  is present in the FOV, i.e.  $x_n^j \in (0, L_x]$ , then its pixel coordinates in image  $n$  is  $(m_{x_n}^j, m_{z_n}^j)$ , where  $m_{x_n}^j = \lceil \frac{x_n^j}{\Delta x} \rceil$ ,  $m_{x_n}^j \in [l_x]$  ( $\lceil a \rceil$  is the smallest integer larger than  $a$ ) and since coordinates  $z$  remain unchanged over time we set  $z_1^j, \forall j \in [N_P]$ , to have the form

$$z_1^j = z_n^j = (m_{z_n}^j - \frac{1}{2})\Delta z, \quad (2)$$

$m_{z_n}^j \in [l_z]$ . Further, we select the row index

$$i_n^j = (n-1)l_x l_z + m_{z_n}^j l_x - m_{x_n}^j + 1 \quad (3)$$

and define the entries in the  $j$  column of the dictionary as

$$D_{ij} = D_{ij}(v_m) = \begin{cases} 1, & \text{if } i = i_n^j, \\ 0, & \text{otherwise.} \end{cases} \quad (4)$$

We stress the fact that, with all discretization parameters fixed, a dictionary  $D$  of particle trajectories corresponding to a single velocity profile (1) is parametrized by the single scalar maximal velocity  $v_m$ .

The above definition implies that the number of non vanishing entries in any column  $j$  does not exceed the number of images  $N_I$ . This is consistent with the physical picture that a particle appears only once in a measured image, or it does not appear at all. We note that two columns  $D_{\bullet,j}, D_{\bullet,j'}$  will be equal if and only if the initial coordinates for two different particles are equal, i.e.  $(x_1^j, z_1^j) = (x_1^{j'}, z_1^{j'})$ . Consequently  $D$  will not contain redundant (equal) columns. Another consequence is the orthogonality of the columns of  $D$ , as formally stated next.

**Proposition 1.** For any two columns  $D_{\bullet,j}$  and  $D_{\bullet,j'}$  in  $D$  corresponding to particles with initial coordinates  $(x_1^j, z_1^j)$  and  $(x_1^{j'}, z_1^{j'})$  we have

$$\langle D_{\bullet,j}, D_{\bullet,j'} \rangle = 0 \iff (x_1^j, z_1^j) \neq (x_1^{j'}, z_1^{j'}). \quad (5)$$

**Proof.** We show  $\langle D_{\bullet,j}, D_{\bullet,j'} \rangle \neq 0 \iff (x_1^j, z_1^j) = (x_1^{j'}, z_1^{j'})$ .

" $\Leftarrow$ " Clear, in view of (1) and the construction of  $D$ .

" $\Rightarrow$ " Assume  $\langle D_{\bullet,j}, D_{\bullet,j'} \rangle \neq 0$ . We show that this implies  $(x_1^j, z_1^j) = (x_1^{j'}, z_1^{j'})$ . The assumption implies that there exists an index  $i_n = i_{n'}$  such that  $D_{i_n j} = D_{i_n j'} = 1$ , i.e. by (3)

$$n l_x l_z + m_{z_n}^j l_x - m_{x_n}^j = n' l_x l_z + m_{z_{n'}}^{j'} l_x - m_{x_{n'}}^{j'}. \quad (6)$$

From  $m_{z_n}^j = \{1, \dots, l_z\}$  and  $m_{x_n}^j = \{1, \dots, l_x\}$ , we have  $0 \leq m_{z_n}^j l_x - m_{x_n}^j \leq l_x l_z - 1$ , and similarly for  $j'$ , i.e.  $0 \leq m_{z_{n'}}^{j'} l_x - m_{x_{n'}}^{j'} \leq l_x l_z - 1$ . Dividing (6) through  $l_x l_z$ , we get

$$\underbrace{n}_{\in \mathbb{N}} + \underbrace{\frac{m_{z_n}^j l_x - m_{x_n}^j}{l_x l_z}}_{\in [0,1) \cap \mathbb{Q}} = \underbrace{n'}_{\in \mathbb{N}} + \underbrace{\frac{m_{z_{n'}}^{j'} l_x - m_{x_{n'}}^{j'}}{l_x l_z}}_{\in [0,1) \cap \mathbb{Q}} \quad (7)$$

from which we conclude  $n = n'$  and  $m_{z_n}^j l_x - m_{x_n}^j = m_{z_{n'}}^{j'} l_x - m_{x_{n'}}^{j'}$ . Rewriting the latter expression as

$$m_{z_n}^j = m_{z_{n'}}^{j'} + (m_{x_n}^j - m_{x_{n'}}^{j'})/l_x, \quad (8)$$

we infer  $m_{x_n}^j - m_{x_{n'}}^{j'} = 0$  as follows: The relation  $|m_{x_n}^j - m_{x_{n'}}^{j'}| \leq l_x - 1$ ,  $m_{z_n}^j, m_{z_{n'}}^{j'} \in \mathbb{N}$  and  $n = n'$  implies  $m_{x_n}^j = \lceil \frac{x_n^j}{\Delta x} \rceil$ . Since this equality must hold for any  $\Delta x$ , we conclude  $x_n^j = x_{n'}^{j'}$ .

As a consequence, (8) implies  $m_{z_n}^j = m_{z_{n'}}^{j'}$  and hence  $z_1^j = z_1^{j'}$  by (2). This together with (1) and  $x_n^j = x_{n'}^{j'}$  finally implies  $x_1^j = x_1^{j'}$ .  $\square$

### 3.2 Variational Motion Estimation

Given noisy measurements  $F$  of particles  $\{(x_n^j, z_n^j)\}_{j \in [N_P], n \in [N_I]}$  for a collection of  $N_I$  subsequent frames at points of time  $\tau_n = (n-1)\Delta t$ ,  $n \in [N_I]$ , we set up an adaptive variational approach for localizing these particles in  $F$ .

To this end, we exploit the motion model (1) that describes particles' trajectories parametrized by the *unknown maximal velocity*  $v_m$  and *unknown initial coordinates*  $(x_1^j, z_1^j)$ . Aggregating potential local detections over time in this way is our approach (i) to suppress noise, (ii) to discriminate particles from each other, and (iii) to estimate the unknown velocity  $v_m$  that is the ultimate goal from the viewpoint of the application area.

We make the reasonable assumption of knowing an interval

$$v_m \in [v_{\min}, v_{\max}], \quad v_{\min} > 0 \quad (9)$$

that contains the unknown parameter  $v_m$ . Every velocity value  $v'_m \in [0, v_{\max}]$  defines a dictionary  $D(v'_m)$  by (4) that exhaustively enumerates trajectories generated by (1) with  $v_m = v'_m$ , that could have been observed in the image sequence. If we knew the true velocity  $v_m$ , we could detect trajectories in the data  $F$  by sparsely matching  $D(v_m)u$  to  $F$ , where  $u$  corresponds to a sparse indicator vector selecting active trajectories in  $D(v_m)$ .

Since  $v_m$  is not given, we have to estimate it from the data  $F$  as well. Since a single dictionary  $D(v'_m)$  is quite large, setting up a collection of dictionaries

$$D(v) := (D(v_1), D(v_2), \dots, D(v_d)), \quad 0 < v_1 < v_2 < \dots < v_d < v_{\max} \quad (10)$$

with closely spaced values  $\{v_i\}_{i \in [d]}$  is computationally infeasible. We therefore limit  $d$  to a reasonable value (see Section 5 for the setup) and *estimate*  $v_m$  *by an adaptive sequence of dictionaries* defined by a sequence of velocity vectors

$$D_{(k)} := D(v^{(k)}), \quad v^{(k)} = (v_1^{(k)}, \dots, v_d^{(k)})^\top \in [v_{\min}, v_{\max}]^d, \quad k \in \mathbb{N} \quad (11)$$

that localizes  $v_m \in [v_1^{(k)}, v_d^{(k)}]$  in intervals of shrinking sizes:  $|v_d^{(k)} - v_1^{(k)}| < |v_d^{(k-1)} - v_1^{(k-1)}|$ . At each iterative step  $k$ , we match trajectories and data by solving

$$u^{(k)} := \underset{u \in [0, 1]^N}{\operatorname{argmin}} \|D_{(k)}u - F\|_1 + \frac{\alpha}{2} \|u\|^2 + \frac{1}{2\lambda} \|u - u^{(k-1)}\|^2, \quad \alpha > 0, \lambda > 0. \quad (12)$$

We stress that nonnegativity constraints enforce *sparse recovery* without explicit sparse regularization [10]. In order to additionally cope with *sparse outliers* we decided to use an  $\ell_1$ -based data/linear model discrepancy term, since minimizing  $\|D_{(k)}u - F\|_1$  is better suited for sparse error recovery, see [11]. Subsequently, we subdivide  $u^{(k)}$  into subvectors conforming to the structure (10) of  $D_{(k)}$ ,

$$u^{(k)} = (u^{1,(k)}, \dots, u^{d,(k)}), \quad (13)$$

and estimate  $v_m$  as convex combination of the velocity values  $v^{(k)}$  defining the current dictionary  $D_{(k)}$ ,

$$v_m^{(k)} := \sum_{i \in [d]} w_i^{(k)} v_i^{(k)} = \langle w^{(k)}, v^{(k)} \rangle, \quad w_i^{(k)} := \frac{1}{\|u^{(k)}\|_1} \|u^{i,(k)}\|_1, \quad i \in [d]. \quad (14)$$

Iteration step  $k$  is completed by updating the velocity vector

$$v^{(k+1)} = V_\tau(u^{(k)}, v^{(k)}), \quad v_i^{(k+1)} := v_m^{(k)} + \tau(v_i^{(k)} - v_m^{(k)}), \quad i \in [d], \quad (15)$$

with  $\tau \in (0, 1)$ . In the next section, it is shown that for any choice of the parameters  $\lambda > 0$  and  $\tau \in (0, 1)$ , the sequence of *non-stationary* mappings (i.e. depending on  $k$ )

$$v^{(k)} \xrightarrow{\text{Eqn. (12)}} u^{(k)} \xrightarrow{\text{Eqn. (15)}} v^{(k+1)} \quad (16)$$

is a fixed point iteration that converges to a constant vector  $v^{(\infty)} = v_m \mathbb{1}$ , that constitutes the estimate of  $v_m$ . The quality of this estimate from the applied viewpoint as outlined in Section 2, will be assessed in Section 5.

## 4 Convergence Analysis

We next show the convergence of the scheme (16) under mild conditions. The proof reveals how the scheme can be modified from the viewpoint of the intended application without compromising convergence. We describe a promising variant in the next paragraph.

**Convergence.** We write for the proximal mapping  $u^{(k-1)} \rightarrow u^{(k)}$  defined by (12)

$$u^{(k)} = P_\lambda f(u^{(k-1)}, v^{(k)}) := \operatorname{argmin}_u f(u, v^{(k)}) + \frac{1}{2\lambda} \|u - u^{(k-1)}\|^2, \quad (17a)$$

$$f(u, v^{(k)}) := \|D_{(k)}u - F\|_1 + \frac{\alpha}{2} \|u\|^2 + \delta_C(u), \quad C = [0, 1]^N, \quad (17b)$$

$$e_\lambda f(u, v^{(k)}) := \inf_w f(w, v^{(k)}) + \frac{1}{2\lambda} \|w - u\|^2, \quad (17c)$$

in order to exhibit the parametrization by  $v^{(k)}$  defining the dictionary (11). Eq. (17c) additionally introduces the Moreau envelope  $e_\lambda f$  of  $f$  [12, Def. 1.22], that we need in the proof of Prop. 2 below.

Likewise, we regard the mapping  $v^{(k)} \mapsto v^{(k+1)}$  defined by (15) as parametrized by  $u^{(k)}$ . These mutual dependencies of the sequences  $(u^{(k)})_{k \in \mathbb{N}}$  and  $(v^{(k)})_{k \in \mathbb{N}}$  and their convergence are addressed next.

**Proposition 2.** *Let the sequences  $(u^{(k)})_{k \in \mathbb{N}}$ ,  $(v^{(k)})_{k \in \mathbb{N}}$  be given by (12) and (15), respectively. Suppose the mapping  $v \mapsto D(v)$  is continuous. Then, for any initializations  $v^{(0)} \in [v_{\min}, v_{\max}]^d \subset \mathbb{R}_{++}^d$  and  $u^{(0)} \in C$ , the sequence  $v^{(k)} \xrightarrow{k \rightarrow \infty}$*

$v^{(\infty)} = v_m^{(\infty)}\mathbb{1}$  converges to a constant vector as fixed point, and the sequence  $u^{(k)} \xrightarrow{k \rightarrow \infty} u^{(\infty)} = \operatorname{argmin} f(u, v^{(\infty)})$  converges to the corresponding minimizer of  $f$ .

*Proof.* The mapping (15) reads in view of (14)

$$V_\tau(u, v) = \tau v + (1 - \tau)v_m\mathbb{1} = (\tau I + (1 - \tau)\mathbb{1}w^\top(u))v =: V_\tau(u)v. \quad (18)$$

We observe for every fixed  $u \in C$ :

- (i)  $w(u) \in \Delta_d$  and hence constant vectors  $c\mathbb{1}$ ,  $c > 0$ , constitute fixed points:  $V_\tau(u)(c\mathbb{1}) = \tau c\mathbb{1} + (1 - \tau)\langle w(u), c\mathbb{1} \rangle \mathbb{1} = c\mathbb{1}$ .
- (ii) The matrix  $V_\tau(u)$  has eigenvalues  $\tau \in (0, 1)$  with multiplicity  $d - 1$  and 1, where the constant vectors are the eigenvectors corresponding to the largest eigenvalue 1.

As a consequence,  $V_\tau$  constitutes a contraction for any non-constant vector  $v$ ,  $\|V_\tau(u, v') - V_\tau(u, v)\| < \|v' - v\|$ , independent of  $u$ . Conversely, if we fix any feasible  $v$  and consider any sequence  $u^{(k)} \rightarrow u$ , then we have  $V_\tau(u^{(k)}, v) \rightarrow V_\tau(u, v)$  due to the continuity of  $V_\tau(\cdot, v)$ .

As a consequence of these properties, a variant of Banach's fixed point theorem [13, Prop. 1.2] asserts that the equation  $v_u = V_\tau(u, v_u)$  has exactly one positive solution in the unit sphere  $(S^{d-1} \cap [v_{\min}, v_{\max}]^d) \subset \mathbb{R}_{++}^d$  and that  $v_{u^{(k)}} \rightarrow v_u$ .

Next, we consider the mapping  $u^{(k-1)} \mapsto u^{(k)}$ , given by the proximal mapping (17), that is parametrized by  $v^{(k)}$ . We have to show convergence of the sequence of minima (17a), which is best covered by the epi(graphical)-convergence [12, Def. 7.1] of the sequence (17b) of functions  $f^{(k)} := f(\cdot, v^{(k)})$ , whose analysis simplifies due to  $f$  being proper, lower semicontinuous and (strongly) convex as follows.

By [12, Thm. 7.37], pointwise convergence  $e_\lambda f^{(k)}(u) \rightarrow e_\lambda f^{(\infty)}(u)$  of the Moreau envelopes (17c) for some  $\lambda > 0$ , which holds due to the continuity of  $v \mapsto D(v)$  by assumption, already yields epi-convergence of the sequence  $f^{(k)}$  to  $f^{(\infty)}$ . This in turn assures by [12, Thm. 7.33] convergence of the unique minima  $u^{(k)} \rightarrow u^{(\infty)}$ , where uniqueness is due to the strict convexity of the objective function of (17a), and finally  $u^{(\infty)} = \operatorname{argmin} f^{(\infty)}$ .  $\square$

As a result, the sequence  $v^{(k)}$  converges to a constant vector  $v^{(\infty)} = v_m\mathbb{1}$  in connection with the convergence of minima  $u^{(k)} \mapsto u^{(\infty)}$  that finally determines the constant  $v_m$  which is the estimate we are primarily interested in, by matching the dictionary  $D(v^{(\infty)})$  to the given data  $F$  through minimizing  $\|D(v^{(\infty)})u - F\|_1$ .

*Remark 1.* The assumption of continuity of the mapping  $v \mapsto D(v)$ , made in Prop. 2, does not strictly hold true for our current implementation described in Section 3.1, but only “up to (small) discretization effects”. Our experiments show however that this does not compromise convergence. A more refined discretization using smooth compactly supported basis functions will remove this (minor) deficiency in our future work.

**Variants of the Estimation Scheme.** The proof of Proposition 2 shows that the assertion holds for any smooth mapping

$$u^{(k)} \mapsto w^{(k)} = w(u^{(k)}) \in \Delta_d. \quad (19)$$

As a consequence, we can investigate alternatives to the mapping (14). Attractive candidates are mappings that are more sensitive to the subvector  $u^{i,(k)}$  in (13) with maximal support  $\max_{i \in [d]} \|u^{i,(k)}\|_1$ . A natural candidate for such a smooth mapping is

$$w_i^{(k)} := \frac{1}{\sum_{j \in [d]} e^{s_j/\varepsilon}} e^{s_i/\varepsilon}, \quad s_i := \|u^{i,(k)}\|_1, \quad \varepsilon > 0, \quad i = 1, 2, \dots, d. \quad (20)$$

This results in a strictly positive vector  $w^{(k)} \in \Delta_d$  that, for  $\varepsilon \rightarrow 0$ , concentrates its mass at the component  $i \in [d]$  corresponding to  $\max_{i \in [d]} \|u^{i,(k)}\|_1$ .

We summarize the performance of this variant in numerical experiments in Section 5.

## 5 Numerical Experiments

In this section, we illustrate the performance of our approach (see Section 3 and Alg. 1 below, for a compact summary), in noisy and non-noisy environments.

**Experimental Setup.** The experimental verification was done using data simulated as follows.

- (a) first, randomly distribute a fixed number of microbubbles in the cross section of a tube with length  $L$  (100cm) and radius  $R$  (5cm);
- (b) select an arbitrary value for  $v_m^*$  between  $v_{min} = 0.001$  and  $v_{max} = 5$ ;
- (c) calculate the position of every microbubble according to Eq. (1) at each time step  $\tau_n = (n - 1)\Delta t$ ,  $\Delta t = 0.2s$ ;
- (d) scan simultaneously the field of view  $\Omega = [0, L_x] \times [0, L_z]$  at each time  $\tau_n$  and store  $N_I = 20$  binary 2D images of size  $l_x \times l_z$  (in pixels) and microbubbles position therein.  $L_x = L_z = 10$  cm and  $l_x = l_z = 100$ ;
- (e) sort all  $N_I$  images and form the larger image  $F_{ideal} =: F$  of size  $l_x \times N_I l_z$  (see Figure 4);
- (f) add noise to mimic ghost particles or error in the position of particles in the form of outliers or perturbing positions in a random direction of random particles. The amount of noise is given by

$$\# \text{ fraction of corrupted entries} = \frac{\|F_{ideal} - F_{noise}\|_1}{2\|F_{ideal}\|_1}.$$

We set the particle density to 10 particles/cm. For practical reasons we precompute and store in advance dictionary blocks corresponding to a single velocity profile for all velocity values in  $[v_{min}, v_{max}]$  in steps of  $\Delta v = 0.001$ . The velocity resolution on this particular grid is of the order of  $\Delta v$ . Thus dictionary blocks  $D(v_1)$  and  $D(v_2)$  corresponding to  $v_1$  and  $v_2$  coincide if  $|v_1 - v_2| < \Delta v$ .

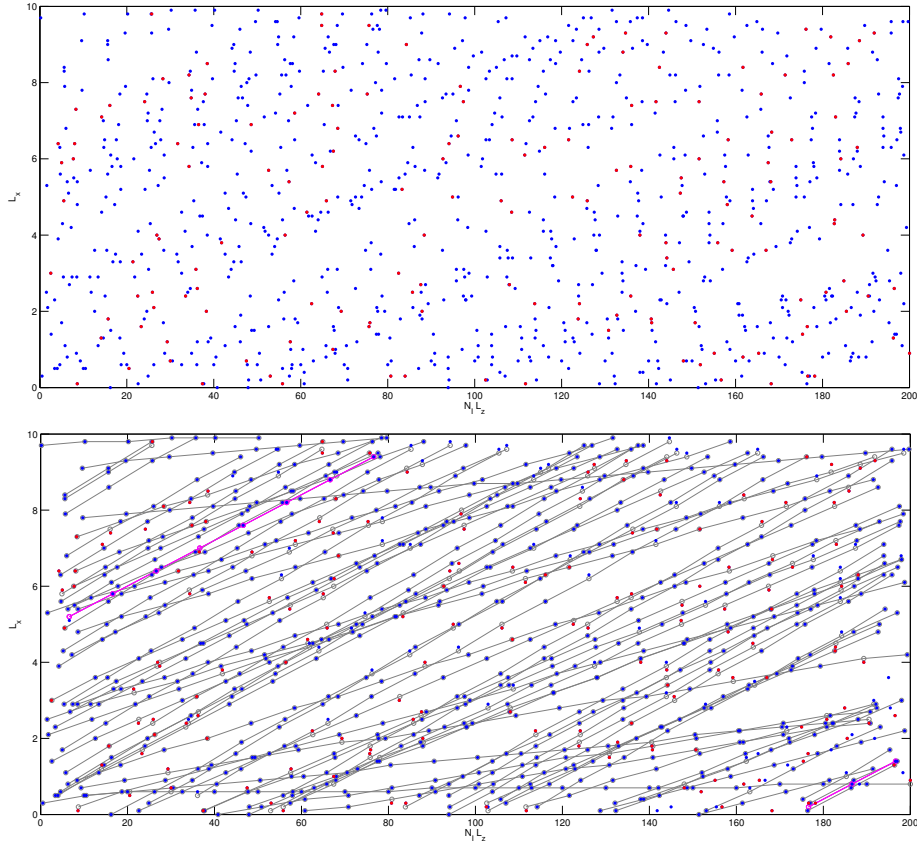


**Fig. 4.** Typical input (top) and output (bottom) of Alg. 1, but here using only 1% of the actual particle density for the purpose of visualization (better viewed in color). 20% (red dots) of input data are corrupted. All points should ideally belong to 84 unknown trajectories. Our proposed algorithm assigns microbubbles in the input frames to particle trajectories from a sparsifying dictionary. Correctly matched trajectories are displayed by thin black lines, wrong ones with magenta. The slopes of matched trajectories yield the velocity of each particle. Quantitative performance statistics for the full data sets are listed in Table 1.

**Optimization.** For the two proposed variants mapping velocities (according to (14) or (20)), we run Alg. 1 below until the accuracy  $\Delta v$  was reached. The large-scale optimization task of Alg. (1) is the application of the proximal mapping and solving (12) at each iteration. To perform this task we currently use the CVX package for *disciplined convex programming* [14]. The average runtime for solving (12) is 5 minutes. Currently each  $D$  is a *highly sparse*  $(2 \cdot 10^5) \times (N_P(v_i^k) \cdot d) \approx 2 \cdot 10^5 \times 10^6$  matrix, with  $d = 11$  and  $i \in [d]$ . Each  $N_P$  depends on each velocity value  $v_i^k$  and  $N_P(v_i^k) < l_x l_z + (N_I - 1) \Delta t v_i^k l_x L_x / l_z = 10^5 + 38v_i^k$ . For processing real data a dedicated numerical optimization algorithm is necessary as CVX cannot

---

**Algorithm 1:** Fixed Point Algorithm with two variants of mapping velocities according to (14) or (20).

---

**Data:** concatenated frames  $F$ ,  $d \in \mathbb{N}$  initial estimates for velocity profiles  $v^{(1)} = (v_1^{(1)}, \dots, v_d^{(1)})$ , parameters  $\Delta v > 0$ ,  $\lambda > 0$ ,  $\alpha > 0$ ,  $\varepsilon > 0$ ,  $\tau \in (0, 1)$

**Result:**  $v_m, N_P$

$k = 1$  ;

**while**  $|v_d^{(k)} - v_1^{(k)}| < \Delta v$  **do**

$D_{(k)} = (D(v_1^{(k)}), D(v_1^{(k)}), \dots, D(v_d^{(k)}))$ ;

$u^{(k)} = \arg \min_{u \in [0,1]} \|D_{(k)} u - F\|_1 + \frac{\alpha}{2} \|u\|^2 + \frac{1}{2\lambda} \|u - u^{(k-1)}\|^2$  ;

Compute weights from (14) / (20) ;

$\forall j \in [d]: w_j^{(k)} = \frac{s_j}{\|u^{(k)}\|_1}$ ,  $s_j := \|u^{j,(k)}\|_1$  /  $w_j^{(k)} := \frac{1}{\sum_{\ell \in [d]} e^{s_\ell/\varepsilon}} e^{s_j/\varepsilon}$ ;

$v_m^{(k)} = \sum_{i \in [d]} w_i^{(k)} v_i^{(k)}$ ;

$\forall j \in [d]: v_j^{(k+1)} = v_m^{(k)} + \tau(v_j^{(k)} - v_m^{(k)})$ ;

$k = k + 1$ ;

$v_m = v_m^{(k)}$ ,  $N_P = \|u^{(k)}\|_0$ ;

---

handle much larger problem sizes. We emphasize that by ignoring the quadratic terms in (12) the problem can be recast as a linear program. Thus (12) can be seen as a perturbed linear program. Our future work from the algorithmic point of view will exploit this fact along with the structure and sparsity of  $D$  consisting of  $d$  building blocks having each orthogonal columns due to Proposition 1.

**Results and Discussion.** Fig. 4 illustrates the detection and particle trajectories after convergence to the fixed point according to Prop. 2. The convergence behavior is depicted by Fig. 5 along with a discussion in the caption. Finally Fig. 6 demonstrates a remarkable robustness of our approach against data noise over a wide range of values of the parameters  $\tau \in (0, 1)$ ,  $\lambda > 0$  and  $\varepsilon$  in (20), due to the aggregation of all information over the entire spatio-temporal volume.

## 6 Conclusion

We have reformulated the velocity estimation problem for a steady laminar flow via Echo PIV as a sparse and global spatio-temporal estimation problem, using a physical flow model. The input data was the whole image sequence assumed to be well approximated by the sum of few elements from a flow dictionary. Since the dictionary was parametrized by the unknown velocity profile, we updated the dictionary in each iteration, thereby refining the unknown quantity. We showed convergence to a fixed point of the overall scheme under weak assumptions to a sparsifying dictionary that robustly estimated velocity even in the presence of high levels of noise. Numerical examples demonstrated this robustness, convergence and estimation accuracy of our approach.

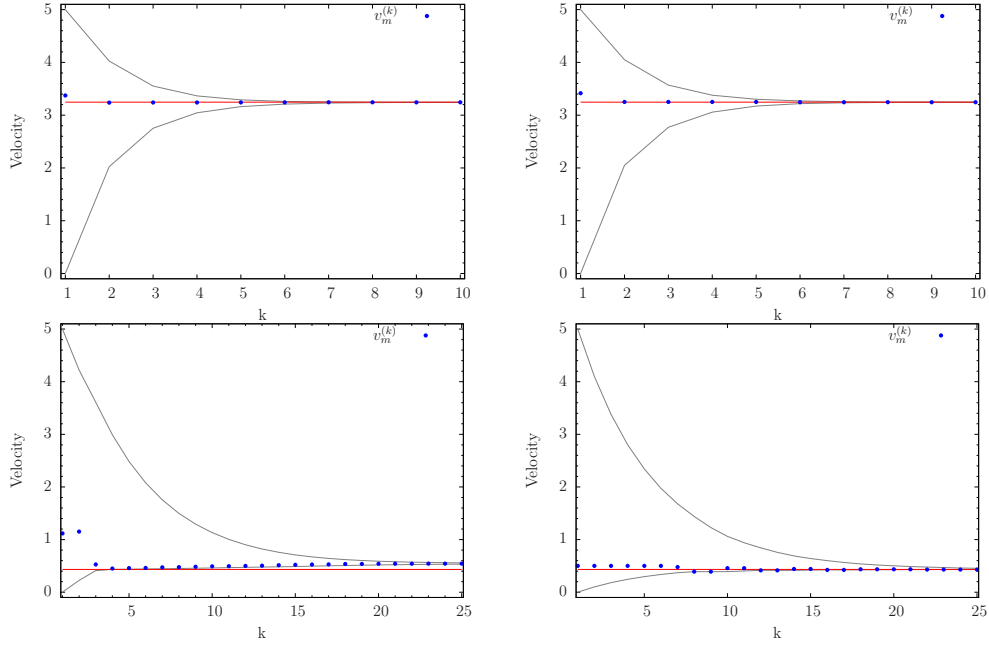


**Fig. 5.** Convergence performance of the fixed point Alg. 1 and its two variants for 20% noise, for *large* ( $v_m^* = 3.2463$ , top row) and *small* true (unknown) velocity ( $v_m^* = 0.4321$ , bottom row). Both variants of the algorithm for estimating  $v_m^*$  converged in 10 (top) and 25 (bottom) iterations. However, computing the weights  $w_i$  according to (20) based on the softmax function – *softmax-weights* – (right) leads to a more accurate estimate of  $v_m^*$  than computing weights according to (14) – *l<sub>1</sub>-weights* – (left). Further numerical values are given in Table 1 based on averaged results over 20 runs.

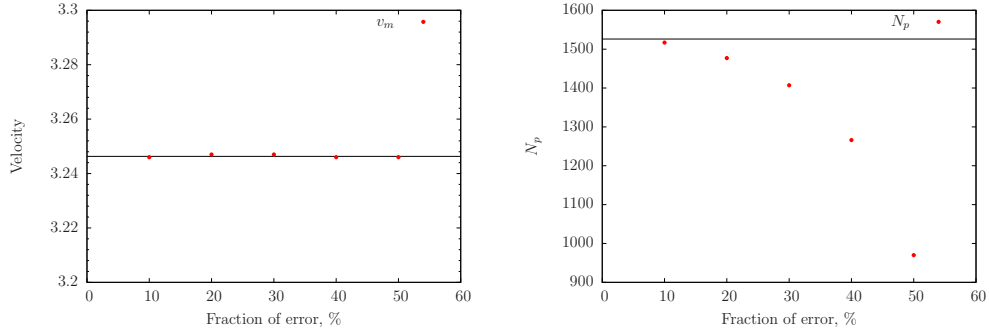


**Fig. 6.** Estimating the velocity  $v_m^*$  via Alg. 1 is robust (left) to corrupting a large fraction of the input data, although the fraction of correctly detected trajectories decreases (right). This fraction suffices to define a “correct” dictionary  $D(v^{(k)})$  due to the convergence of  $v^{(k)}$  to a uniform vector  $v_m \mathbb{1}$ . Results are consistent for different values of  $\tau \in [0.4, 0.8]$ ,  $\tau \in [0.2, 0.4]$  and  $\varepsilon \in \{50, 100, 150, 200\}$ .

$v_m^* = 3.2463; N_p^* = 1526; \tau = 0.4$						
0 %		10 %		20 %		
	$v_m$	$N_p$	$v_m$	$N_p$	$v_m$	$N_p$
$\ell_1$ -weights	$3.2437 \pm 0.003$	1526	$3.2438 \pm 0.0003$	$1513 \pm 3$	$3.2437 \pm 0.005$	$1478 \pm 8$
softmax-weights	$3.2450 \pm 0.006$	1526	$3.2456 \pm 0.007$	$1519 \pm 3$	$3.2460 \pm 0.0006$	$1493 \pm 5$
$v_m^* = 0.4321; N_p^* = 1035; \tau = 0.8$						
0 %		10 %		20 %		
	$v_m$	$N_p$	$v_m$	$N_p$	$v_m$	$N_p$
$\ell_1$ -weights	$0.4416 \pm 0.016$	1031	$0.4688 \pm 0.0037$	$754 \pm 11$	$0.5291 \pm 0.0227$	$360 \pm 64$
softmax-weights	$0.4300 \pm 0.020$	1035	$0.4296 \pm 0.0007$	$1032 \pm 2$	$0.4299 \pm 0.0008$	$731 \pm 24$

**Table 1.** Estimated velocity and number of particles for ideal and noise data. The velocity value to be estimated is  $v_m^*$ . The number of true trajectories is  $N_p^*$ . We averaged results over 20 runs. Velocity estimates are stable against noise, and the results reveal better estimates for the softmax-weights in the case of small velocities.

Further work will concentrate on adapting the dictionary using more general physical fluid flow models, and incorporating models of the real imaging sensor with proper discretization.

## References

- Kim, H., Hertzberg, J., Shandas, R.: Development and Validation of Echo PIV. *Exp. Fluids* **36**(3) (2004) 455–462
- Poelma, C., van der Mijle, R.M.E., Mari, J.M., Tang, M.X., Weinberg, P.D., Westerweel, J.: Ultrasound Imaging Velocimetry: Toward Reliable Wall Shear Stress Measurements. *European Journal of Mechanics - B/Fluids* **35** (2012) 70–75
- Raffel, M., Willert, C., Wereley, S., Kompenhans, J.: Particle Image Velocimetry – A Practical Guide. Springer (2007)
- Schiffner, M.F., Schmitz, G.: Fast Image Acquisition in Pulse-Echo Ultrasound Imaging using Compressed Sensing. In: *Ultrasonics Symposium (IUS), 2012 IEEE International, IEEE* (2012) 1944–1947
- Rodriguez, S., Jacob, X., Gibiat, V.: Plane Wave Echo Particle Image Velocimetry. In: *Proceedings of Meetings of Acoustics, POMA 19.* (2013)
- Womersley, J.: Method for the calculation of velocity, rate of flow and viscous drag in arteries when the pressure gradient is known. *J. Physiol.* **127** (1955) 553–563
- Sutera, S., Skalak, R.: The History of Poiseuille’s Law. *Ann. Rev. Fluid Mech.* **25** (1993) 1–19
- Adrian, R.J.: Twenty Years of Particle Image Velocimetry. *Experiments in Fluids* **39**(2) (2005) 159–169
- Westerweel, J.: Fundamentals of Digital Particle Image Velocimetry. *Measurement Science and Technology* **8**(12) (1997) 1379–1392
- Slawski, M., Hein, M.: Sparse Recovery by Thresholded Non-Negative Least Squares. In: *Proc. NIPS.* (2011) 1926–1934
- Candès, E.J., Tao, T.: Decoding by Linear Programming. *IEEE Transactions on Information Theory* **51**(12) (2005) 4203–4215
- Rockafellar, R., Wets, R.J.B.: *Variational Analysis.* 2nd edn. Springer (2009)
- Zeidler, E.: *Nonlinear Functional Analysis and its Applications: Fixed Point Theorems. Volume I.* Springer (1993)
- Grant, M., Boyd, S.: CVX: Matlab Software for Disciplined Convex Programming, version 2.1. <http://cvxr.com/cvx> (March 2014)